Replies to Editor comments/suggestions

Editor Decision: Publish subject to technical corrections (02 March 2021) by Dr. Rolf Müller

Comments to the Author: Dear authors, congratulations to your paper which is accepted for ACP. Please take into account the technical corrections.

Reply: We thank you very much for getting through review and appreciating the actual content of the work.

P27L463: "4. Summary and conclusions" start a new line.

Reply: Corrected.

P28L488: →Figs. 3 and 4

Reply: Corrected.

---END---

Structure, dynamics, and trace gases variability within the Asian summer monsoon anticyclone in extreme El Niño of 2015-16

Saginela Ravindra Babu[1 *], Madineni Venkat Ratnam[2], Ghouse Basha[2], Shantanu Kumar Pani[1] and Neng-Huei Lin[1,3*]

[1]Department of Atmospheric Sciences, National Central University, Taoyuan 32001, Taiwan

[2]National Atmospheric Research Laboratory, Gadanki 517112, India.

[3]Center for Environmental Monitoring and Technology, National Central University, Taoyuan 32001, Taiwan

*Correspondence to: S.Ravindra Babu (baburavindra595@gmail.com) and N.-H. Lin (nhlin@cc.ncu.edu.tw)

Abstract: A weak El Niño during 2014-15 boreal winter was developed as a strong boreal summer event in 2015 which continued and even enhanced during the following winter. In this work, the detailed changes in the structure, dynamics and trace gases within the Asian summer monsoon anticyclone (ASMA) during extreme El Niño of 2015-16 is delineated by using Aura Microwave Limb Sounder (MLS) measurements, COSMIC Radio Occultation (RO) temperature, and NCEP reanalysis products. Our analysis concentrates only on the summer months of July and August 2015 when Nino 3.4 index started to exceed 1.5 values. The results show that the ASMA structure was quite different in summer 2015 as compared to the long-term (2005-2014) mean. In July, the spatial extension of the ASMA shows larger than the long-term mean in all the regions except over northeastern Asia, where, it exhibits a strong southward shift in its position. The ASMA splits into two and western Pacific mode is evident in August. Interestingly, the subtropical westerly jet (STJ) shifted southward from its normal position over northeastern Asia as resulted mid-latitude air moved southward in 2015. Intense Rossby wave breaking events along with STJ are also found in July 2015. Due to these dynamical changes in the ASMA, pronounced changes in the ASMA tracers are noticed in 2015 compared to the long-term mean. A 30% (20%) decrease in carbon

monoxide (water vapor) at 100 hPa is observed in July over most of the ASMA region, whereas in August the drop is strongly concentrated in the edges of the ASMA. Prominent increase of O_3 (>40%) at 100 hPa is clearly evident within the ASMA in July, whereas in August the increase is strongly located (even at 121 hPa) over the western edges of the ASMA. Further, the temperature around the tropopause shows significant positive anomalies (~5K) within the ASMA in 2015. The present results clearly reveal the El Niño induced dynamical changes caused significant changes in the trace gases within the ASMA in summer 2015.

Keywords: Trace gases, El Niño, Asian summer monsoon anticyclone, tropopause

1. Introduction

The Asian summer monsoon anticyclone (ASMA) is a distinct circulation system in the upper troposphere and lower stratosphere (UTLS) during northern hemisphere boreal summer, centered at ~25^{o}N and extending roughly between 15^{o}N to 40^{o}N (Park et al., 2004; Randel et al., 2010). It is encircled by the subtropical westerly jet stream to the north and by the equatorial easterly jet to the south (Randel and Park, 2006). It is well recognized that the ASMA circulation is a prominent transport pathway for troposphere pollutants to enter the stratosphere (Randel et al., 2010). Previous studies have concluded that deep convection during summer monsoon can effectively transport the pollutants, aerosols and tropospheric tracers from the boundary layer into the UTLS region (Vogel et al., 2016; Santee et al., 2017). These transported pollutants, tracers and aerosols become confined in the ASMA and, consequently, affect the trace gas composition in the UTLS region (Randel et al., 2010; Solomon et al., 2010; Riese et al., 2012; Hossaini et al., 2015). It is clearly evident from the previous studies that the ASMA has a higher concentrations of tropospheric tracers such as carbon monoxide (CO), hydrogen cyanide (HCN) and Methane (CH_4) and lower concentrations of stratospheric tracers including Ozone (O_3) and nitric acid (HNO_3)

(Park et al., 2004; Li et al., 2005; Park et al., 2008; Randel et al., 2010; Vernier et al., 2015; Yan and Bian, 2015; Yu et al., 2017; Santee et al., 2017; Vernier et al., 2018). The comprehensive study on the climatological composition within the ASMA can be found in Santee et al. (2017). The ASM convection and orographic lifting are the primary mechanisms for the higher concentrations of the tropospheric tracers in the ASMA (Li et al., 2005; Park et al., 2009; Santee et al., 2017). Apart from these trace gases a strong persistent tropopause-level aerosol layer called as 'Asian Tropopause Aerosol Layer' (ATAL) also existed between 12 to 18 km within the ASMA and it was first detected from the CALIPSO measurements (Vernier et al., 2011).

Similarly, higher concentrations of water vapor (WV) within the ASMA during the summer monsoon is well documented in the literature (Gettelman et al., 2004; Park et al., 2007; Randel et al., 2010; Bian et al., 2012; Xu et al., 2014; Jiang et al., 2015; Das and Suneeth, 2020). It is well known that most of the WV enters the stratosphere through the tropical tropopause (Fueglistaler et al., 2009) and the temperature presented at the tropical tropopause strongly controls the WV entering the lower stratosphere (LS). It is also well documented that several processes such as convection, strength of the Brewer-Dobson circulation, El Niño–Southern Oscillation (ENSO) and Quasi-Biennial Oscillation (QBO) are responsible for the WV transport to the UTLS region (Holton et al., 1995; Dessler et al., 2014; Jiang et al., 2015). Other factors such as gravity waves and horizontal advection can also influence the WV transport in the UTLS region. For example, Khan and Jin (2016), studied the effect of gravity waves on the tropopause and WV over Tibetan Plateau and reported that the gravity wave is the source for the WV transport from the lower to higher altitudes. Recently, Das and Suneeth (2020) reported about the distributions of WV in the UTLS over the ASMA during summer using 13 years of Aura Microwave Limb Sounder observations. They concluded that WV in the UTLS region inside the central part of ASMA is

86 mostly controlled by horizontal advection and very less from the local process and tropopause
87 temperature in both summer and winter.

88 Convection during the summer monsoon is one of the major sources to transport the boundary
89 layer pollutants into the UTLS region (Randel et al., 2010). It is well established fact that the ENSO
90 has a strong influence on convection and circulation changes over the Asian monsoon region
91 (Kumar et al., 1999; Wang et al., 2015; Gadgil and Francis, 2016). Enhanced (suppressed)
92 convection over the Asian monsoon region generally observed in the cold phase of ENSO (warm
93 phase of ENSO) known as La Niña (El Niño). Few studies have existed to date on the impact of
94 ENSO on the ASMA trace gas composition changes and its dynamical changes. For example, Yan
95 et al. (2018) reported the influence of ENSO on the ASMA with a major focus on how the ENSO
96 winter signal propagates into the following seasons. They showed the weaker O_3 transport into the
97 tropics during the onset of the ASMA after boreal winter El Niño events, but the difference between
98 El Niño and La Niña composites becomes insignificant in the summer. In another study, Tweedy
99 et al. (2018) demonstrated the impact of boreal summer ENSO events on O_3 composition within
100 the ASMA in different phases of ENSO events. They reported that the ASMA forms earlier and
101 stronger in the La Niña period that leads to greater equatorward transport of O_3-rich air from the
102 extra-tropics into the northern tropics than during El Niño periods. Recently, Fadnavis et al. (2019)
103 reported higher concentrations of aerosol layers observed in the ATAL region during the El Niño
104 period over the northern part of South Asia. However, the above- mentioned studies are mainly
105 focused on changes in the ASMA with respect to ENSO on seasonal scales or mature stage of
106 monsoon (combined mean of July and August).

107 Based on the above-mentioned studies, it can be concluded that the ENSO also has a strong
108 influence on the ASMA structure and its composition. The recent 2015-16 El Niño event was

109 recorded as an extreme and long-lasting event in the 21st century (Huang et al., 2016; Avery et al.,
110 2017). It was started as a weak El Niño during 2014-15 boreal winter and it developed as a strong
111 boreal summer El Niño event in 2015 (Tweedy et al., 2018). Further, this strong boreal summer
112 event was continued and significantly enhanced until the boreal winter of 2015-16. In this event,
113 several unusual changes occurred in the tropical UTLS region including, the strong enhancement
114 in the lower stratosphere WV (higher positive tropopause temperature anomalies) over Southeast
115 Asia and western Pacific regions (Avery et al., 2017) and anomalous distribution of trace gases in
116 the UTLS region (Diallo et al., 2018; Ravindra Babu et al., 2019a). Similar way, the response of
117 different trace gases (O_3, HCl, WV) to the disrupted 2015–2016 quasi-biennial oscillation (QBO)
118 associated with 2015-16 El Niño event is also reported by Tweedy et al. (2017). Dunkerton (2016),
119 discussed the possible role of unusual warm ENSO event in 2015-2016 to the QBO disruption by
120 triggering the extratropical planetary waves. Therefore, in the present study, we investigated the
121 detailed changes observed in the ASMA 2015 particularly by focusing on the structure, dynamics
122 and trace gases variability within the ASMA in July and August 2015 by using satellite
123 observations and reanalysis products. The present research article is organized as follows.
124 Database and methodology adopted in this study are discussed in Section 2. The results and
125 discussions are illustrated in Section 3. Finally, the summary and conclusions obtained from the
126 present study are summarized in Section 4.

127 **2. Database and Methodology**

128 **2.1. Microwave Limb Sounder (MLS) measurements**

129 In the present study, version 4.2 Aura MLS measurements of CO, O_3 and WV are utilized.
130 The MLS data of July and August months in each year from 2005 to 2015 period are considered.
131 The vertical resolution for CO is in the range 3.5–5 km from the upper troposphere to the lower

mesosphere and the useful range is 215–0.0046 hPa. The horizontal resolution for CO is about 460 km at 100 hPa and 690 km at 215 hPa. For WV, the vertical resolution is in the range of 2.0 to 3.7 km from 316 to 0.22 hPa and the along-track horizontal resolution varies from 210 to 360 km for pressure greater than 4.6 hPa. For O_3, the vertical resolution is ~2.5 km and the along-track horizontal resolution varies between 300 and 450 km. The precision (systematic uncertainty) for WV is ~ 10-40% (~10-25%), for O_3 is ~0.02–0.04 (~0.02–0.05) ppmv and for CO, it is ~ 19 ppbv (30%), respectively. More details about the MLS version 4 level 2 data can be found in Livesey et al. (2018).

2.2. COSMIC Radio Occultation measurements

To see the changes in the tropopause temperature and height within the ASMA, we used high-resolution, post-processed products of level 2 dry temperature profiles obtained from Constellation Observing System for Meteorology, Ionosphere, and Climate (COSMIC) Radio Occultation (RO). Each month of July and August from 2006 to 2015 are considered. The data is downloaded from the COSMIC Data Analysis and Archival Center (CDAAC) website. We used 200 m vertical resolution temperature profiles in the study. Details of the temperature retrieval from the bending angle and refractivity profiles obtained from the RO sounding are presented well in the literature (Kursinski et al. 1997; Anthes et al. 2008). The COSMIC temperature have a precision of 0.1% between 8 and 25 km (Kishore et al. 2009; Kim and Son, 2012). The temperature accuracy in the UTLS is better than 0.5 K for individual profiles and ~0.1 K for averaged profiles (Hajj et al. 2004). It is noted that for individual RO temperature profiles, the observational uncertainty estimate is 0.7 K in the tropopause region, slightly decreasing into the troposphere and gradually increasing into the stratosphere (Scherllin-Pirscher et al., 2011a). For monthly zonal-averaged temperature fields, the total uncertainty estimate is smaller than 0.15 K in the UTLS (Scherllin-

Pirscher et al., 2011b). Overall, the uncertainties of RO climatological fields are small compared to any other UTLS observing system for thermodynamic atmospheric variables. Note that these data are compared with a variety of techniques including GPS radiosonde data and observed good correlation particularly in the UTLS region (Rao et al. 2009; Kishore et al. 2009). The COSMIC RO profiles have been widely used for studying the tropopause changes and its variabilities (Kim and Son, 2012; RavindraBabu et al. 2015; RavindraBabu and Liou, 2021).

2.3. National Centers for Environmental Prediction (NCEP) Reanalysis data

We also utilized monthly mean Geopotential height (GPH) and wind vectors (zonal and meridional wind speed) from the NCEP-DOE Reanalysis 2 (Kanamitsu et al.,2002), covering the same time period as the MLS observations (2005-2015). NCEP-DOE Reanalysis 2 is an improved version of the NCEP Reanalysis I model that fixed errors and updated parametrizations of physical processes. The horizontal resolution of NCEP-DOE Reanalysis 2is 2.5° × 2.5°, respectively.

Apart from the above-mentioned data sets, we also used European Centre for Medium-Range Weather Forecasts (ECMWF) interim reanalysis potential vorticity (PV) data particularly at 350K isentropic surface in July and August 2015 (ERA-Interim; Uppala et al., 2005; Dee et al., 2011).

2.5. Methodology

Daily available MLS profiles of O_3, CO, and WV in each month are constructed and gridded by averaging the profiles inside bins with a resolution of 5° latitude × 5° longitudes. The following equation is used to estimate the relative change in percentage.

$$\text{Relative change in percentage} = \left(\frac{x_{i-\bar{x}}}{\bar{x}}\right) \times 100 \qquad (1)$$

where x_i represents the monthly mean of July/August in 2015, and $\bar{x}$ is the corresponding monthly long-term mean which is calculated by using the data from 2005 to 2014.

3. Results and Discussion

178 It is well reported that the ASMA is highly dynamic in nature with respect to its position and shape.
179 Also it varies at different time scales i.e day-to-day, weekly and monthly scales caused by internal
180 dynamical variability (Randel and Park, 2006; Garny and Randel, 2013; Pan et al., 2016; Nützel
181 et al., 2016; Santee et al., 2017). The intensity and spatial extension of the ASMA are prominent
182 in July and August where the monsoon was in the mature phase (Santee et al., 2017; Basha et al.,
183 2019). It can be noticed that the 2015-16 El Niño event was one of the strongest boreal summer
184 events that occurred in the entire MLS data record (Tweedy et al., 2018). In this event, the Nino
185 3.4 data was exceeded +1.5 in July and +1.8 in August (**Fig. 1**). Therefore, in the present study,
186 we mainly focused on ASMA behavior and trace gases changes within the ASMA on monthly
187 scales particularly in July and August 2015 which represents strong El Niño.

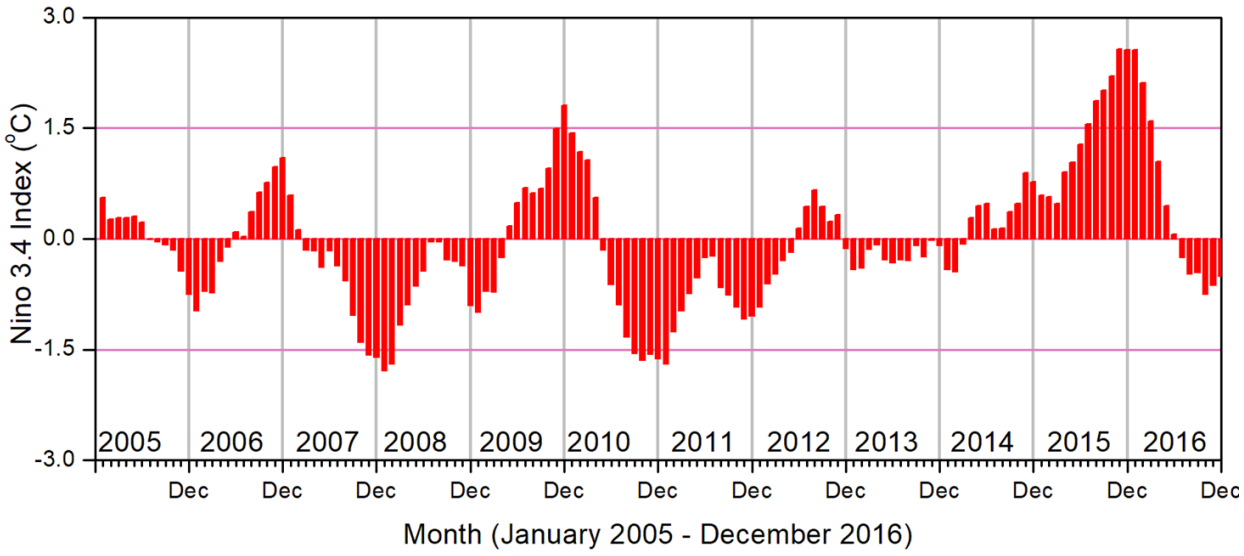

188

189 **Figure 1**. Temporal evolution of observed Niño3.4 Index data from January 2005 to December
190 2016.

191 **3.1. Structure and dynamical changes in ASMA during 2015**

192 In general, the studies looking at monthly or seasonal timescales related to the thermo-
193 dynamical features in the ASMA, the anticyclone region is mostly defined from the simple
194 constant GPH contours at different pressure levels (Randel and Park, 2006; Yan et al., 2011;

Bergman et al., 2013; Basha et al., 2019). Previous researchers used different GPH contours at 100 hPa to define the anticyclone region. For example, Yan et al. (2011) used 16.7 km, Bergman et al. (2013) used 16.77 km and recently Basha et al. (2019) used 16.75 km GPH contour as the anticyclone region. In a similar manner, we also defined the ASMA region based on NCEP-DOE Reanalysis 2 obtained GPH at 100 hPa and considered the 16.75 km GPH contour as the anticyclone region.

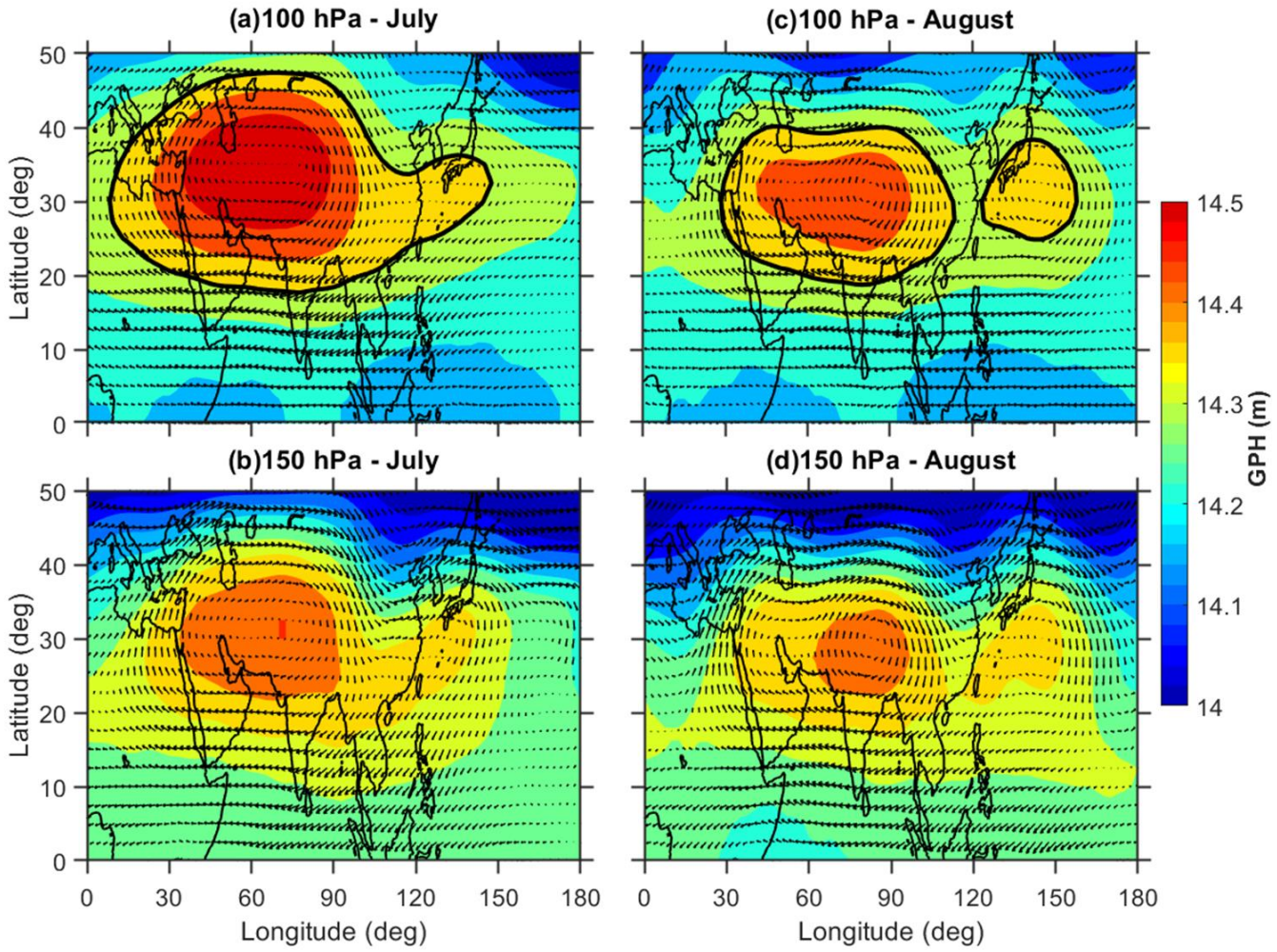

Figure 2. Spatial distribution of geopotential height obtained from NCEP-DOE Reanalysis 2 data during July 2015 (a) at 100 hPa and (b) 150 hPa superimposed with wind vectors at the respective corresponding levels. Subplots of (c) and (d) are the same as (a) and (b) but for the month of August. The black color solid contour lines represent the ASMA region at 100 hPa (16.75 km GPH contour).

The spatial distribution of GPH at 100 hPa and 150 hPa for the month of July (August) is shown in **Fig. 2a and 2b (Fig. 2c and 2d).** The corresponding monthly mean winds at respective pressure levels are also shown in **Fig.2**, respectively. The black solid line represents the ASMA region at 100 hPa based on 16.75 km GPH contour. The GPH distribution in **Fig. 2** shows clear distinct variability in the ASMA spatial structure between July and August at both pressure levels. For example, at 100 hPa, the maximum GPH center was located over western side in July whereas it was located over near to the Tibetan region in August. Interestingly the ASMA itself separated into two anticyclones (16.75 km GPH contour black solid line in the figure) in August compare to July. The center of the small anticyclone was located over the Northwestern Pacific near 140^{o}E with the closed circulation indicated by the wind arrows.

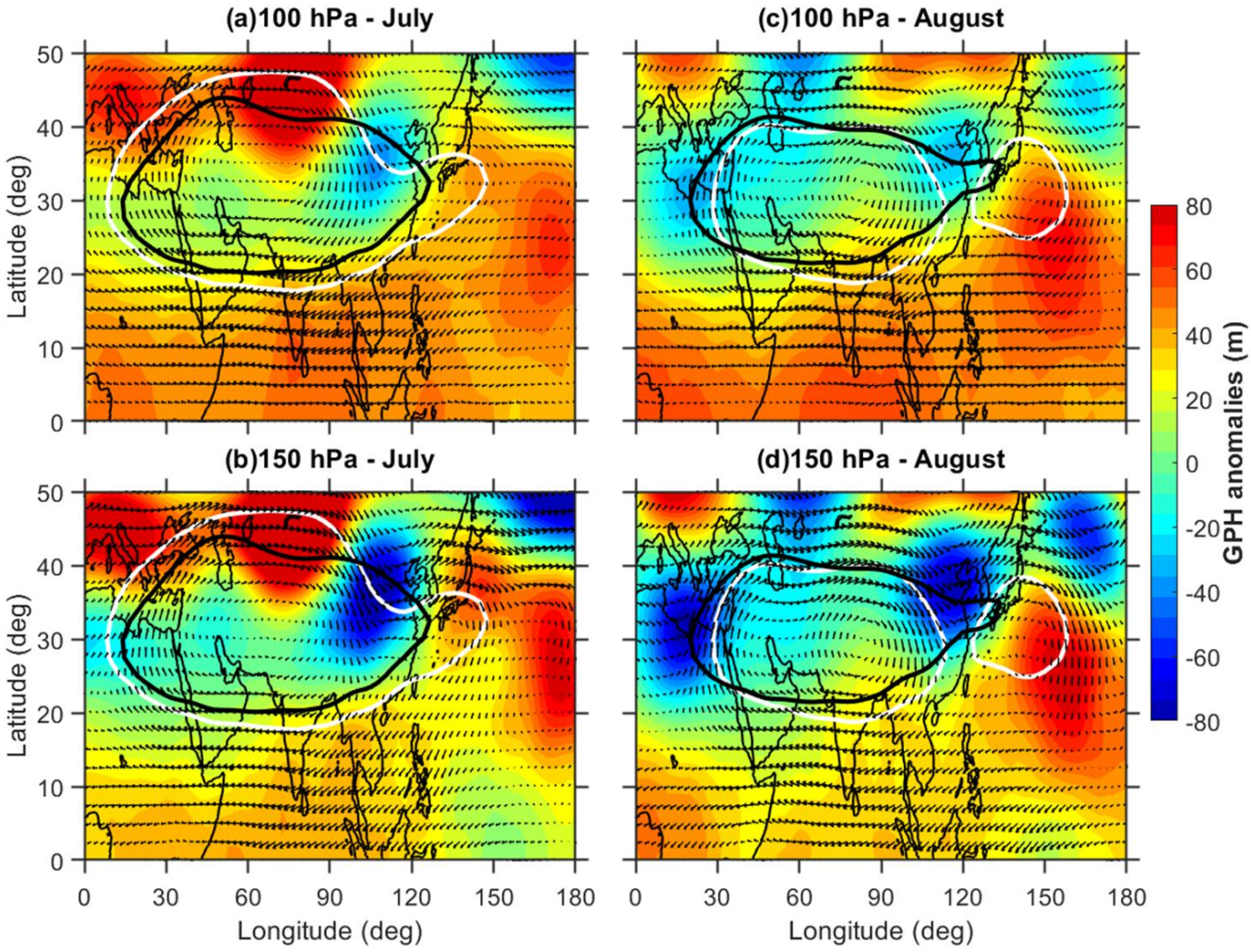

Figure 3. Spatial distribution of geopotential height anomalies obtained from NCEP-DOE Reanalysis 2 data during July 2015 (a) at 100 hPa and (b) 150 hPa superimposed with wind vectors at the respective corresponding levels. Subplots of (c) and (d) same as (a) and (b) but for the month of August. The white color solid contour lines represent the ASMA region at 100 hPa (16.75 km GPH contour) observed in 2015 whereas the black color line represents the mean of 2005-2014.

Further, we compared the ASMA structure in 2015 with referenced long-term mean. For this, we obtained the GPH anomalies by subtracting the background long-term mean (2005-2014) from 2015. **Figure 3** shows the latitude-longitudinal distribution of GPH anomalies (color shaded) along with wind vectors depicting circulation pattern at 100 hPa as well as at150 hPa during July and August. The white (black) color contour represents 16.75 km GPH at 100 hPa for the

corresponding month in 2015 (long-term mean). The GPH anomalies at both pressure levels show quite different features in July and August. A clear wave-like structures can be observed from the GPH anomalies. In July, the GPH anomalies exhibit strong negative maxima over 25-40^{o}N, 90-120^{o}E and positive maxima over 40-50^{o}N, 60-80^{o}E regions. The 16.75 km GPH contour lines in the ASMA region exhibits higher extension in all the directions except over the northeastern edges of the ASMA in July compared to the long-term mean. At the same location (northeastern edges), the ASMA exhibits a pronounced southward extension in July. Distinct features of GPH anomalies are noticed in August as compared to July. In August, the strong negative GPH anomalies are situated over the west and north-eastern edges of the ASMA.

It is well known that the subtropical westerly jet is an important characteristic feature of the ASMA (Ramaswamy 1958), and thus its changes during 2015 are also investigated. As the peak intensity of the westerly jet was located at 200 hPa (Chiang et al., 2015), we focused mainly on 200 hPa zonal wind changes in July and August. **Figure 4a and 4c** (**Fig. 4b and 4d**) show the spatial distribution of long-term (2015) monthly mean zonal wind at 200 hPa during July and August. In general, the subtropical westerlies are located near to ~40^{o}N latitude during the mature phase of the monsoon period (Chiang et al., 2015). Compared to long-term mean, a significant weakening of the subtropical westerlies is noticed in 2015. Further, a strong southward shift in the westerlies is observed over the northeastern Asia region. This southward shift is moved even up to 30^{o}N in both months. From zonal wind at 200 hPa (**Fig. 4**) and wind vectors at 100/150 hPa (**Fig. 2**), it is clear that anomalous changes have occurred in the subtropical westerlies over the northeastern parts of the AMSA around 30-40^{o}N, 90-120^{o}E during July and August 2015. The southward shift in the westerlies is strongly associated with the southward extension of the ASMA over the northeastern side of the ASMA (**Fig. 2**). This is strongly supported by the previous

findings by Lin and Lu (2005) where they showed the southward extension of the South Asian High could lead to the southward shift of the westerlies.

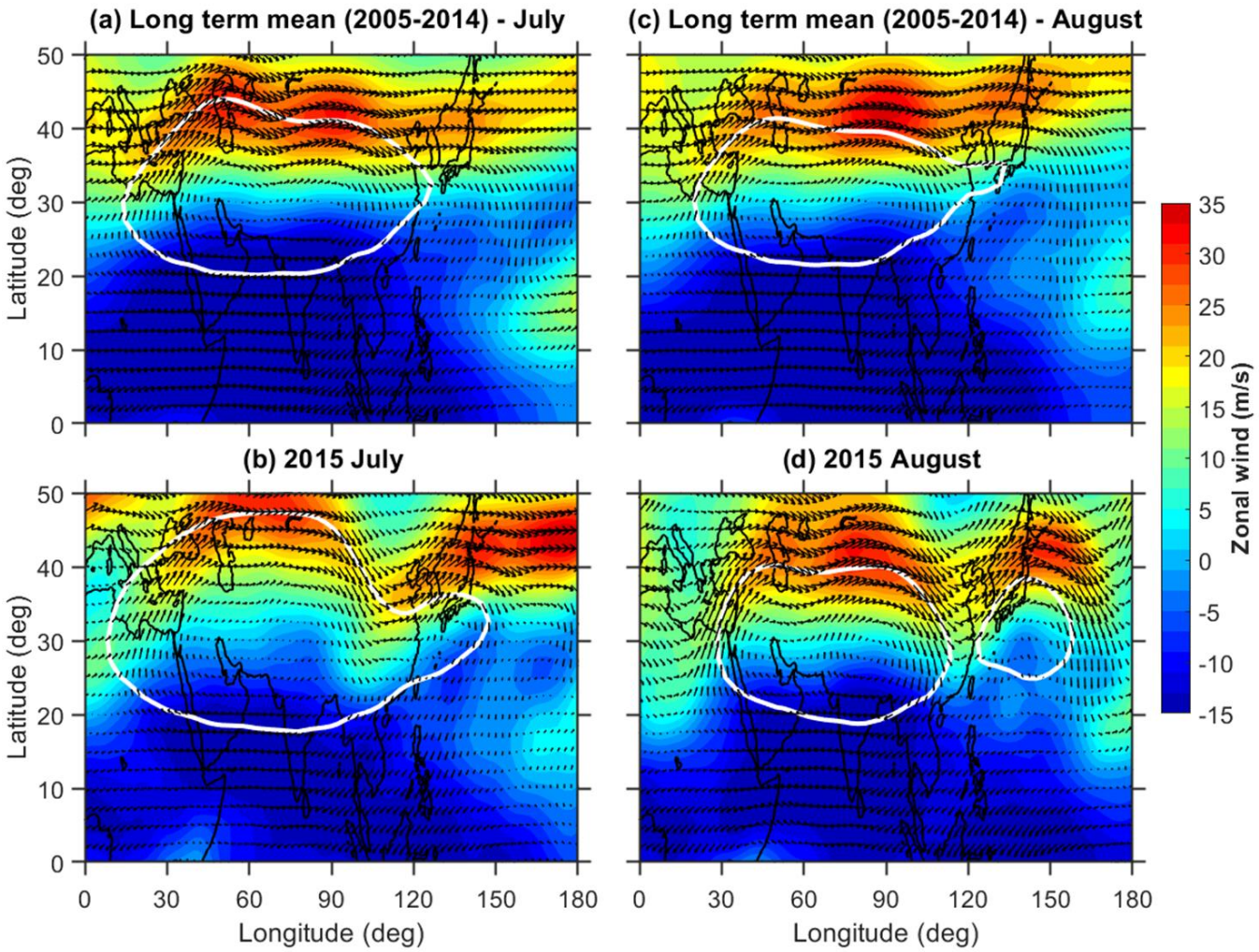

Figure 4. Spatial distribution of monthly mean zonal winds obtained from NCEP-DOE Reanalysis 2 data at 200 hPa during July during (a) 2005-2014 (b) 2015 year. Subplots of (c) and (d) same as (a) and (b) but for the month of August. The white color solid contour lines represent the ASMA region at 100 hPa (16.75 km GPH contour).

From the GPH and winds observations, it is clear that pronounced changes are evident in the dynamical structure of the ASMA in 2015 and also relatively different features are noticed between July and August months. Interestingly the ASMA itself separated into two anticyclones during August 2015 and the separation exactly coincided with the strong negative GPH anomalies

and southward meandering of subtropical westerlies over the northeastern side of the ASMA. The Western Pacific (WP) mode of the anticyclone is visible in August. The split of the anticyclone and the formation of the WP mode are in agreement with previous studies reported by few researchers earlier (e.g. Honomichl and Pan, 2020). The presence of the WP mode may be due to the eastward eddy shedding of the ASMA system in the process of its sub-seasonal zonal oscillation (Honomichl and Pan, 2020) or Rossby wave breaking (RWB) in the subtropical westerly jet (Fadnavis and Chattopadhyay, 2017). Fadnavis and Chattopadhyay (2017) also identified the split of ASMA into two anticyclones: one over Iran and another over the Tibetan region due to the RWB in June 2014 monsoon period. To see any signatures of these RWB in 2015, we further analyzed the RWB through the ERA interim reanalysis potential vorticity (PV) data. Based on previous studies, it is reported that RWBs can be identified from PV distribution at 350 K isentropic surface (Samanta et al. 2016; Fadnavis and Chattopadhyay, 2017). We used 350 K isentropic surface PV data in July and August 2015 in the present analysis.

Figure 5a–b shows the distribution of ERA interim monthly mean PV at the 350 K isentropic surface during July and August 2015. It can be seen that, during July and August 2015, clear RWB signatures evident near 100^{o}E. It is noted that the equatorial advection of high PV values with a steep gradient and the southward movement of PV from the westerly jet are the basic features of the RBW (Vellore et al., 2016; Samanta et al. 2016). These features are clearly exhibited in **Figure 5** with higher PV values extends up to ~ 30^{o}N in both months over 100^{o}E region. The location of this RWB is significantly correlated with a southward meandering of westerlies and strong negative GPH anomalies. However, the observed RWB signatures in both months are from monthly mean PV data. Further, to see the clear signatures of these RWB, we made weekly based analysis for July month. For this we considered 1-7 July as week-1 and 8-14 July as week-2 so on.

The weekly mean distribution of 350K isentropic surface PV during July is shown in **Fig. 6**.

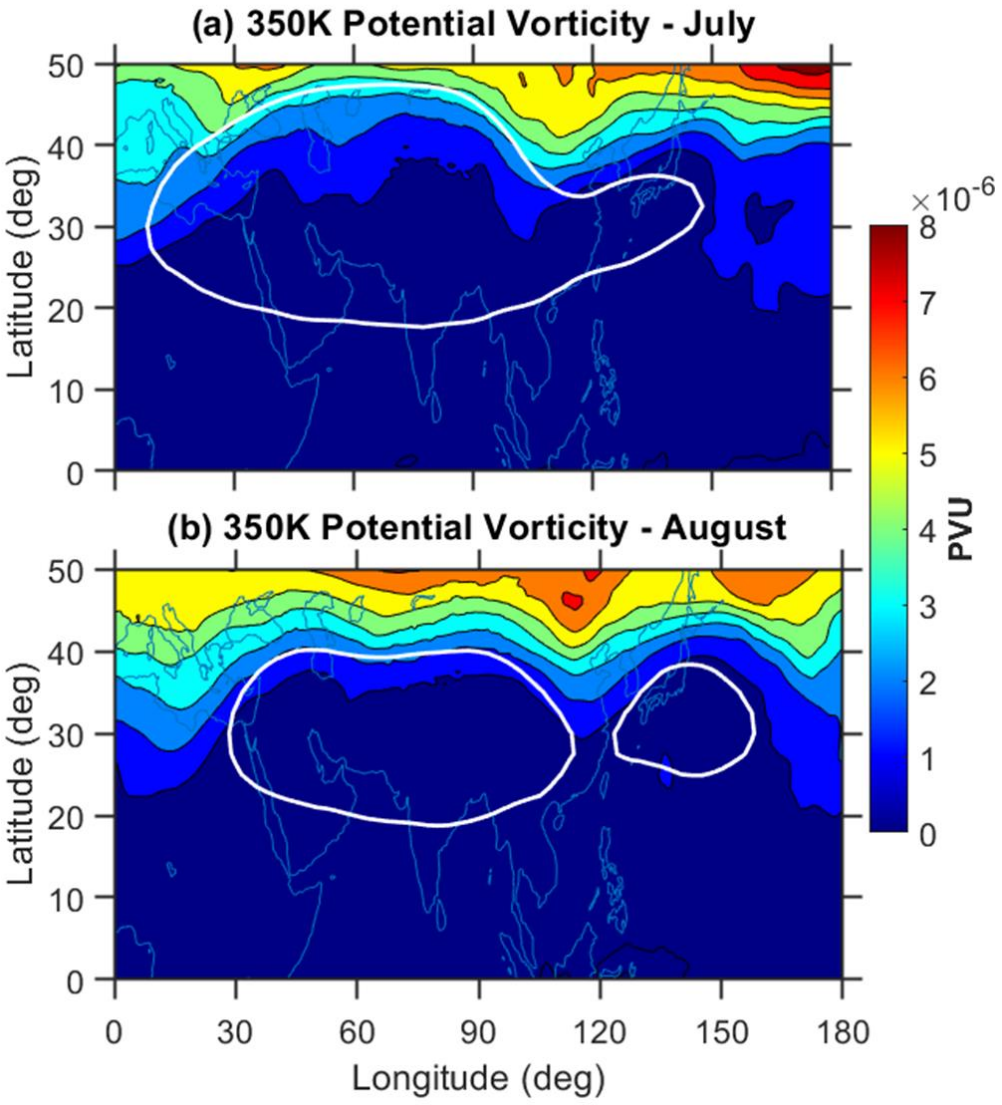

Figure 5. ERA Interim observed spatial distribution of potential vorticity (PV) on a 350 K isentropic surface in PVU (1 PVU = 10^{-6} K m^2 $kg^{-1}s^{-1}$): (a) monthly mean of July and (b) monthly mean of August 2015. The white color solid contour lines represent the ASMA region at 100 hPa (16.75 km GPH contour).

The magenta colored arrows which are shown in the Fig. 6 represents the RBW events during July 2015. A clear signature of air with high values of PV traverses from extra-tropics to ASMA is evident from Fig.6. At weekly scales, clear RWB signatures are observed over the anticyclone region. For example, in week-1 and week-2, the RWB signatures are evident over the northern

region of the ASMA. However, in week-3 and week-4, these RWB signatures are very clear over northeastern Asia even in week-5 (29July-04August), we noticed RWB signatures in PV data (Figure not shown). This clearly shows that The RWB splits the ASMA into two anticyclones: one over the Tibetan region and another over the WP region. It is clear that the equatorward penetration of extra tropical forcing through the subtropical westerly jet has started in July and further amplified by the splitting of the ASMA into two during August.

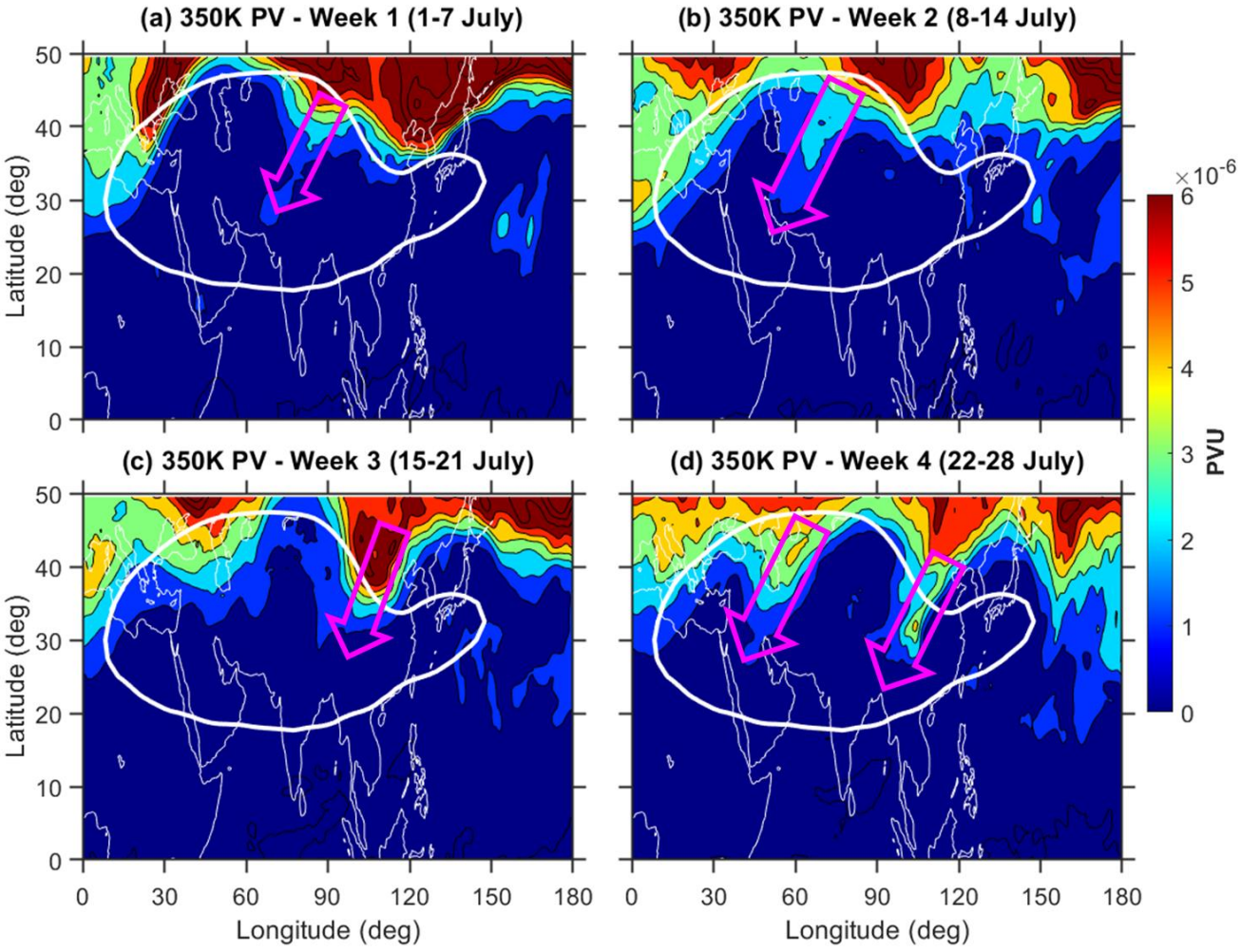

Figure 6. Same as **Figure 5**, but for the weekly distribution of PV in July 2015. Magenta colored arrows indicate the regions of RWB.

It is well known that the RWB is an important mechanism for horizontal transport between the extratropical lower stratosphere to the tropical UTLS region. These RWBs can act as an agent

for the transport of extratropical stratospheric cold, dry, and O_3-rich air into the ASMA during the summer monsoon. Overall, it is concluded that the combination of the RWBs and strong southward meandering of the subtropical westerly jet in 2015 causes significant dynamical and structural changes in the ASMA. These changes in the ASMA dynamical structure in 2015 can influence the concentrations of the different trace gases within the ASMA. Further, we quantified the changes in O_3, CO and WV concentrations within the ASMA during 2015 caused by the dynamical effects. The changes that occurred in the O_3 and CO, WV, are discussed in the following sections.

3.2. Trace gases anomalies observed within the ASMA in 2015

It is well-documented that the ASMA contains low (high) concentrations of stratospheric tracers such as O_3 (tropospheric tracers such as CO, WV and etc.) and higher tropopause height compared to the region outside the ASMA during boreal summer (Park et al., 2007; Randel et al., 2010; Santee et al., 2017; Basha et al., 2019). Differences of the trace gases within and outside of the ASMA are attributed to the strong winds and closed streamlines associated with the ASMA, which act to isolate the air (Randel and Park 2006; Park et al. 2007). To see the changes in the trace gases during 2015, we generated the background long-term mean of CO, O_3, and WV by using 10 years of MLS trace gas data from 2005 to 2014. Here the results are discussed mainly based on the percentage changes relative to the respective long-term monthly mean trace gases using **Equ. 1**.

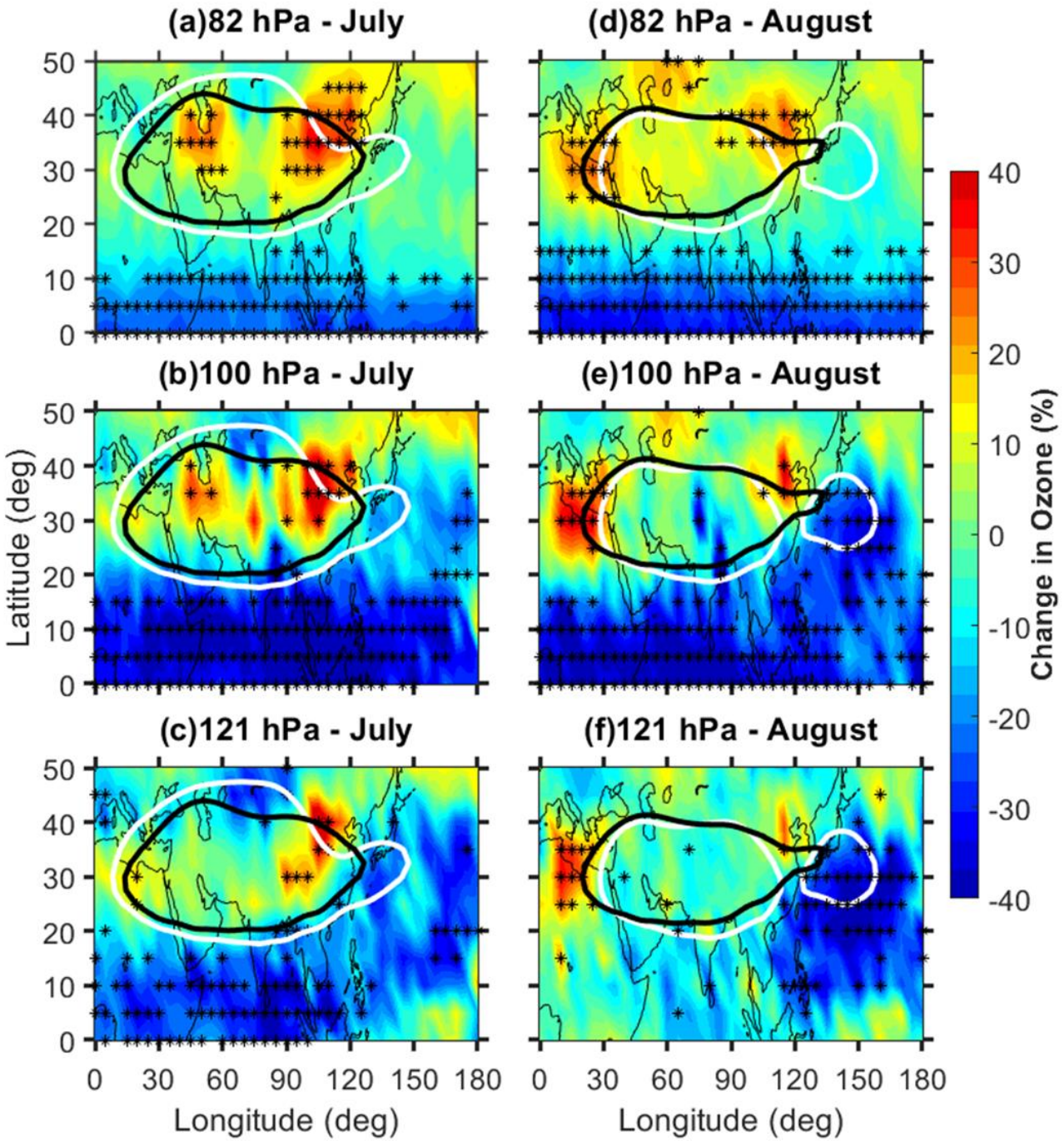

Figure 7. Ozone relative percentage change in July 2015 with respect to background climatological monthly mean observed at (a) 82 hPa, (b) 100 hPa and (c) 121 hPa. Subplots of (d), (e) and (f) same as (a), (b) and (c) but for the month of August. The white (black) color contour represents 16.75 km geopotential height at 100 hPa for the corresponding month in 2015 (mean of 2005-2014). The star symbols (black) shown in figure represent the anomalies greater than the ±2σ standard deviation of long-term mean. The results are obtained from MLS measurements.

Figure 7a-c (**Fig. 7d-f**) shows the distribution of relative percentage change in the O_3 concentrations within the ASMA at 82 hPa, 100 hPa and 121 hPa during July (August) 2015. The anomalies larger than ±2σ standard deviation of long-term mean are highlighted with star symbols in the respective figures. The spatial distribution of changes in the O_3 (Fig. 7) shows a clear increase in the O_3 mixing ratios (>40%) within the ASMA in 2015. The observed increase within the ASMA is quite distinct between July and August. In July, the O_3 shows a pronounced increase within the ASMA at all the pressure levels. Note that the observed increase was statistically significant with larger than 2σ standard deviation of long-term mean (see the star symbols). This increase is quite significant over the northeastern edges of the ASMA and quite high at 100 hPa compared to 82 hPa and 121 hPa. In August, the O_3 shows quite different features compared to July (Fig. 7d-f). A strong increase in the O_3 is observed over the western and eastern edges of the ASMA at all the pressure levels. The increase is quite significant at 100 hPa and even at 121 hPa. The increase of O_3 is still appearing over the northeastern edges of the ASMA in August as observed in July. Overall, a significant enhancement of O_3 within the ASMA is clear evidence in July and August 2015.

The significant increase of O_3 within the ASMA in 2015 might be due to the transport from the mid-latitudes through the STJ and also due to the stratosphere to the troposphere transport. For example, the strong enhancement of O_3 within the ASMA at 100 hPa in July was strongly matched with the observed high values of PV at 350 K isentropic surface (Fig. 6). This is further supported by the strong southward meandering of STJ in July (Fig. 3), respectively. Thus, a clear transport of mid-latitude air with high PV and high O_3 is evident during 2015. At the same time, the enhancement of O_3 was clearly observed at all the pressure levels from 82 hPa to 121 hPa which is further supported for the stratosphere to the troposphere transport. Note that 82 hPa can represent

357 the lower stratosphere and 121 hPa for the upper troposphere (Das et al., 2020). It can be noticed
358 that the ASMA is strongly associated with troposphere-stratosphere transport as well as
359 stratosphere-troposphere transport (Garny and Randel, 2016; Fan et al., 2017). Also, it is well
360 reported that the northern part of the ASMA is an active region for stratosphere-troposphere
361 transport processes (Sprenger et al., 2003; Škerlak et al., 2014).

362 Similarly, significant lowering of O_3, particularly at 100 hPa and 82 hPa is clearly noticed
363 over the tropics (Fig. 7). This is quite expected due to the enhanced tropical upwelling (bringing
364 poor O_3 air from troposphere) caused by the strong El Niño conditions in July and August 2015.
365 As mentioned in the previous sections, strong El Niño conditions are clearly evident in July and
366 August 2015 (Fig. 1). The observed strong negative O_3 anomalies over the tropics from the present
367 study are well matched with the previous studies (Randel et al., 2009; Diallo et al., 2018). From
368 the present results, it is very clear that there is a significant decrease over the tropics and the
369 increase over the mid-latitudes in 2015. These changes observed in the O_3 (decrease and increase)
370 are attributed due to the strengthening of the tropical upwelling and enhanced dowelling from the
371 shallow branch of the Brewer-Dobson circulation in the mid-latitudes due to the strong El Niño
372 conditions in 2015. Overall, it is concluded that initially, during July, the O_3 is transported into the
373 anticyclone from the northeastern edges of the ASMA region through the sub-tropical westerlies
374 and then it is isolated within the ASMA region. This is further supported by the southward
375 meandering of the westerly jet and southward shift of the ASMA (negative GPH anomalies) over
376 the same region in July (**Fig. 3**). Also, significant transport of mid-latitude dry air is clear from the
377 Fig. 6. Thus, it is clear from the results that the stratosphere to troposphere transport and horizontal
378 advection along with the subtropical jet caused the strong enhancement of the O_3 within the ASMA
379 in 2015.

Figure 8a-b (**Fig. 8c-d**) shows the spatial distribution of CO relative percentage change at 100 hPa and 146 hPa observed during July (August) 2015. The white (black) color contour represents 16.75 km GPH at 100 hPa for the corresponding month in 2015 (climatological mean). The observed changes in the CO clearly exhibit quite distinct features between July and August as observed in the O_3. A significant decrease (~30%) is noticed in the CO concentrations over most of the AMSA in July. The maximum decrease of CO is noticed over the northeastern edges of the ASMA, located ~ 30-45^{o}N, 90-120^{o}E region. Whereas in August, the decrease of CO is more concentrated over the east and western edges of the ASMA at both the pressure levels. Overall, the MLS observed CO was ~30% below average (percentage decrease) compared to the climatological monthly mean within the ASMA in July and edges of the ASMA in August 2015. It is noted that there is a considerable year-to-year variability of the CO sources over the ASM region (Santee et al., 2017). The major sources of the CO over the ASM region are from the biomass burning and industrial emission. The observed decreased CO within the ASMA in 2015 might be due to the year-to-year variability in the CO sources and the weaker vertical transport due to the El Niño conditions in 2015.

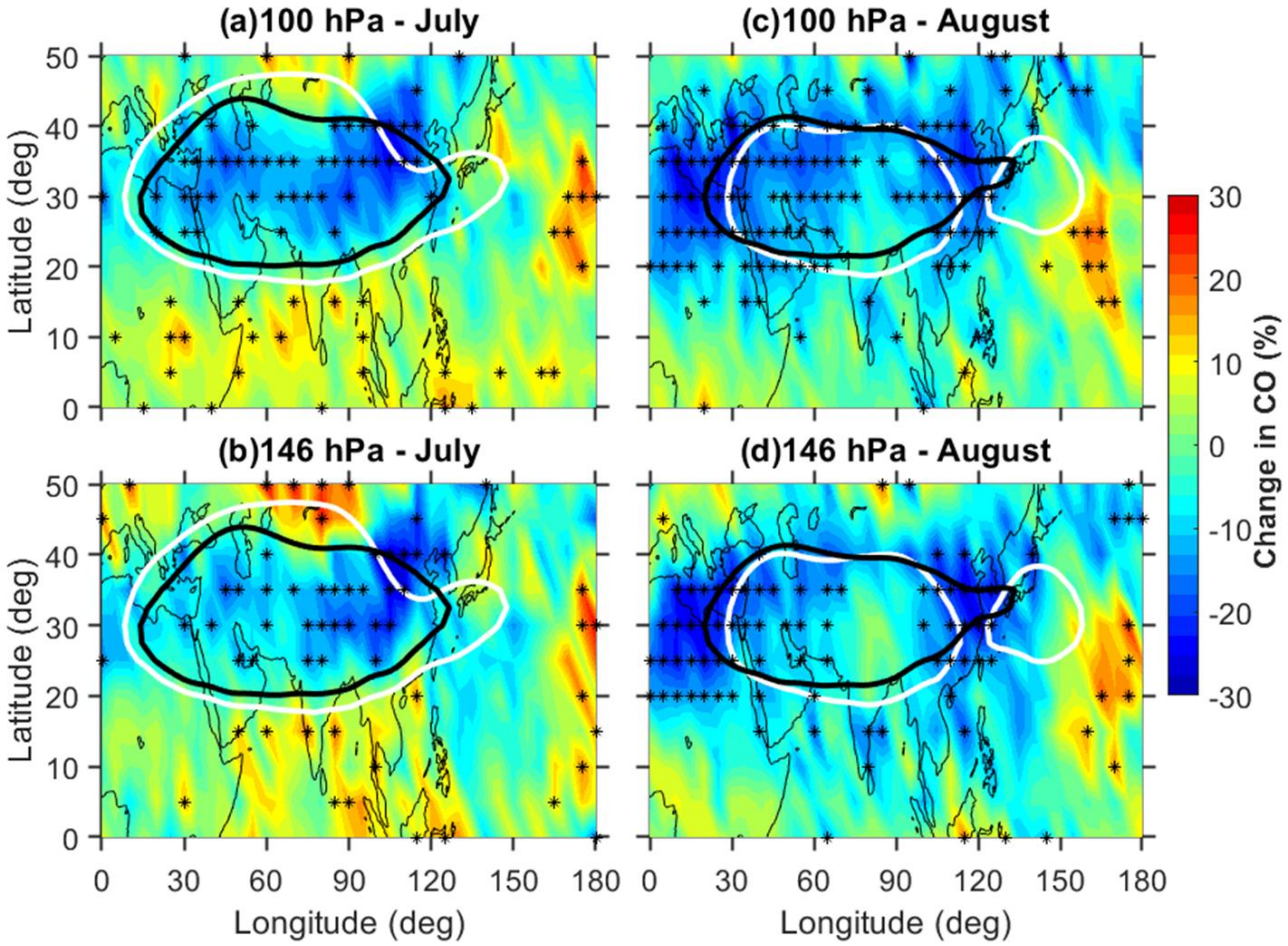

Figure 8. Carbon monoxide relative percentage change during July 2015 with respect to climatological monthly mean observed at (a) 100 hPa and (b) 146 hPa. Subplots of (c) and (d) same as (a) and (b) but for the month of August. The white (black) color contour represents 16.75 km geopotential height at 100 hPa for the corresponding month in 2015 (mean of 2005-2014). The star symbols (black) shown in figure represent the anomalies greater than the ±2σ standard deviation of long-term mean. The results are obtained from MLS measurements.

Similarly, the WV relative percentage change at 82 hPa, 100 hPa and 146 hPa in July (August) 2015 are shown in **Fig. 9a-c** (**Fig. 9d-f**). The WV shows quite different changes at all the pressure levels in July and August. At 146 hPa, the WV exhibits a strong decrease > 20%) within the ASMA in July as well as in August also. However, at 100 hPa and 82 hPa, the WV shows a relatively significant decrease within the ASMA in July compared to August. From the WV observations, it is concluded that the WV is strongly decreased at 146 hPa in both months. Whereas at 100 hPa

and 82 hPa, the decrease in WV is quite high in July compared to August. It is also observed from the Fig. 9 that there is a significant enhancement of WV over the tropics at 146 hPa in both months. But the WV enhancement is quite significant at 100 hPa, particularly during August compared to July. This enhancement in the WV around the tropical tropopause region in August is quite expected due to the El Niño conditions (Randel et al., 2009; Konopka et al., 2016). Overall, the tropospheric tracers (CO and WV) significantly decreased (~30% and 20%) within the ASMA during July and August 2015. These changes in the tropospheric tracers are might be due to the weaker vertical motions during the 2015 monsoon. A weaker vertical transport from the boundary layer to the UTLS is generally observed over the ASM region during El Niño period (Fadnavis et al., 2019). The El Niño conditions will suppress the monsoon convection and cause weaker vertical transport during monsoon. Also it is reported that the summer monsoon in 2015 was weaker monsoon due to the strongest El Niño conditions existed in 2015 (Tweedy et al., 2018; Yuan et al., 2019; Fadnavis et al., 2019).

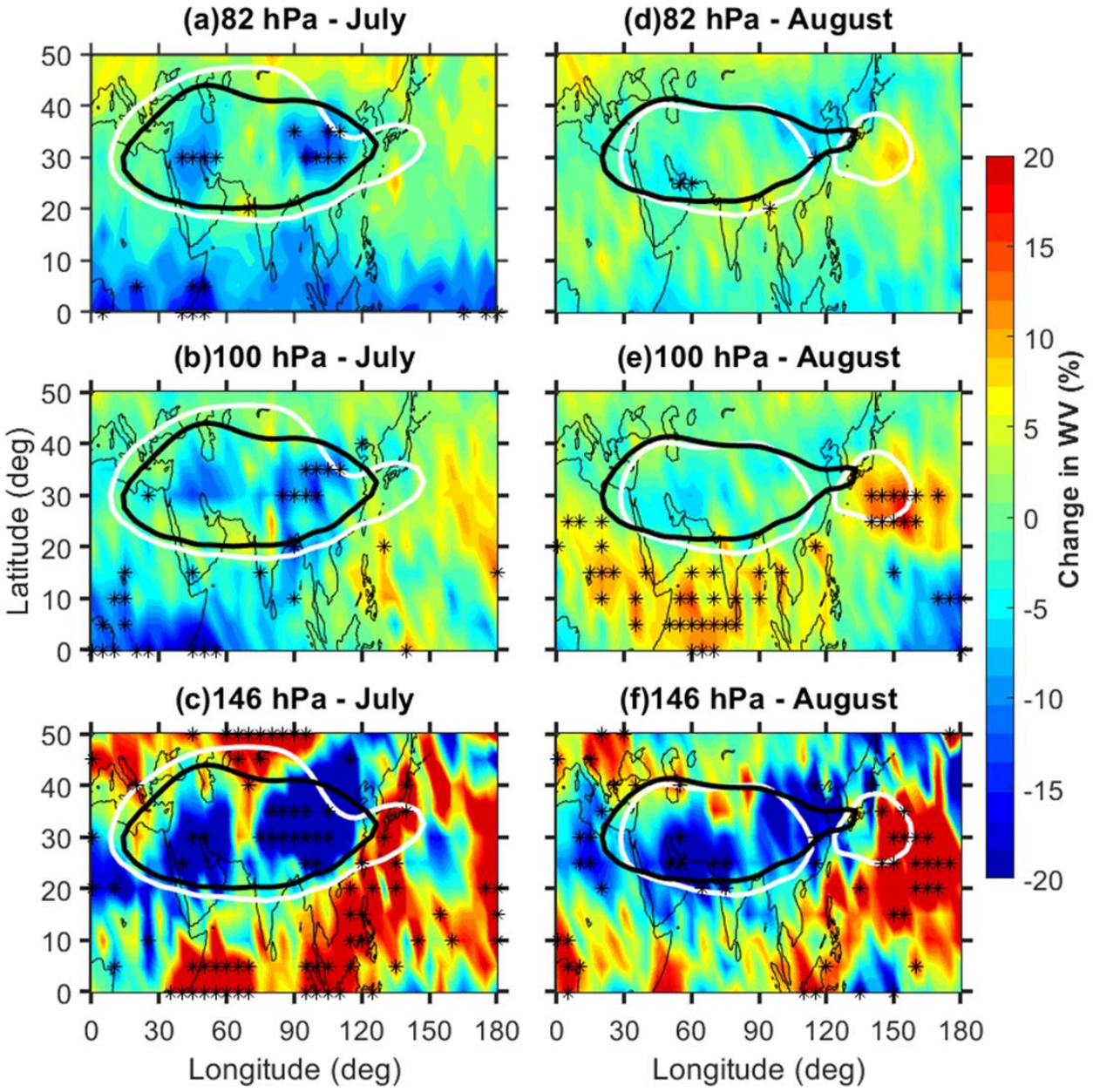

Figure 9. Water vapour relative percentage change in July 2015 with respect to background climatological monthly mean observed at (a) 82 hPa, (b) 100 hPa and (c) 146 hPa. Subplots of (d), (e) and (f) same as (a), (b) and (c) but for the month of August. The white (black) color contour represents 16.75 km geopotential height at 100 hPa for the corresponding month in 2015 (mean of 2005-2014). The star symbols (black) shown in figure represent the anomalies greater than the ±2σ standard deviation of long-term mean. The results are obtained from MLS measurements.

From these results, it is clear that the enhancement of O_3 and lowering of CO/WV is evident in July and August 2015 compared to the long-term monthly mean. The observed high O_3 and low

WV within the ASMA from the present study are consistent and well-matched with the previous study reported by Li et al. (2018). They demonstrated the importance of the large-scale atmospheric dynamics and the stratospheric intrusions for high O_3 and low WV over Lhasa within the ASMA by using in-situ balloon-borne measurements. The O_3/WV changes strongly influence the background temperature structure within the UTLS region (Venkat Ratnam et al., 2016; RavindraBabu et al., 2019b). Further, we investigated the tropopause temperature changes within the ASMA by using COSMIC RO data. The results are presented in the next following section.

3.3. Tropopause temperature anomalies in 2015

It is well known that the tropopause plays a crucial role in the exchange of WV, O_3 and other chemical species between the troposphere and the stratosphere. Most of these exchanges (WV to the lower stratosphere and O_3 to the upper troposphere) known as stratosphere troposphere exchange (STE) take place around the tropopause region (Fueglistaler et al., 2009; Venkat Ratnam et al., 2016; RavindraBabu et al., 2019b). It is well reported that the tropopause within the ASMA is higher than the outside regions at the same latitude (Randel et al., 2010; Santee et al., 2017). In the present study, we mainly focused on changes in the cold point tropopause temperature (CPT) and lapse rate tropopause temperature (LRT) within the ASMA in July and August 2015. The July and August 2015 monthly mean tropopause parameters are removed from the respective climatological monthly mean which is calculated by using COSMIC RO data from 2006 to 2014. One can note that we have strictly restricted our analysis within 40^{o}N region for the cold point tropopause. **Figure 10a-b** (**Fig. 10c-d**) shows the CPT and LRT anomalies observed in July (August) 2015. The tropopause temperature anomalies (CPT/LRT) also exhibit a distinct pattern in July and August as observed in O_3 (**Fig. 7**). In July, the CPT/LRT show strong positive anomalies (~5 K) in most of the ASMA region. High positive CPT/LRT anomalies are also noticed over the

NWP region particularly below 20ºN. These CPT/LRT anomalies observed over the NWP region might be due to the El Niño induced changes in the Walker circulation and convective activity. Previous studies also observed significant warm tropopause temperature anomalies over WP and maritime continent during the El Niño period (Gettleman et al., 2001). In August, the strong positive CPT/LRT anomalies (~5K) are concentrated over the northeastern edges of the anticyclone where the WP mode of the anticyclone was separated from the ASMA. The temperature anomalies at 1 km above and below the CPH also show similar behavior as seen in the CPT/LRT during August 2015 (figures not shown). Overall, the tropopause temperature anomalies in July and August 2015 within the ASMA are well correlated with the strong enhancement in the O_3 as shown in **Fig. 7.** However, the enhanced O_3 anomalies (heating due to the O_3) itself cannot explain the observed positive tropopause temperature anomalies within the ASMA in 2015. This might be due to the El Niño induced changes in the convective activity and the circulation. It is well known that the reversal of walker circulation and the shifting of the convective activity (suppressed convective activity over ASM region) are generally observed during the warm phase of ENSO. One can be noticed that apart from the convection, other factors such as stratospheric QBO, atmospheric waves (gravity waves and Kelvin waves) also strongly influenced the tropopause temperatures.

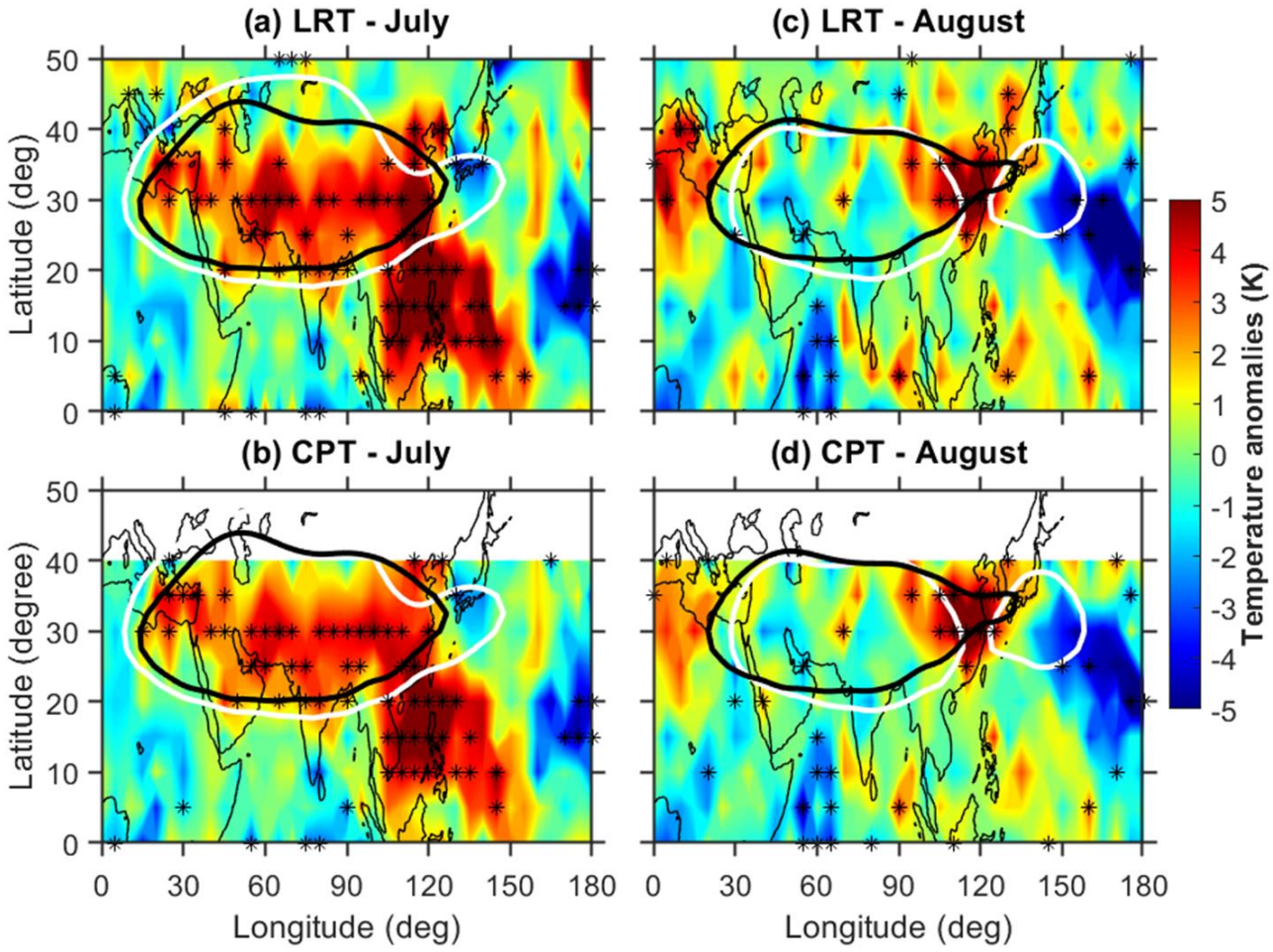

Figure 10. Spatial distribution of (a) lapse rate tropopause temperature (LRT), (b) cold point tropopause temperature (CPT) anomalies during July 2015. Subplots of (c) and (d) same as (a) and (b) but for the month of August 2015. The white (black) color contour represents 16.75 km geopotential height at 100 hPa for the corresponding month in 2015 (mean of 2005-2014). The star symbols (black) shown in figure represent the anomalies greater than the ±2σ standard deviation of long-term mean.

4. Summary and Conclusions

In this study, we investigated the detailed changes observed in the structure, dynamics and trace gases (Ozone, Water Vapor, Carbon Monoxide) variability within the ASMA in 2015 by using reanalysis products and satellite observations. The tropopause temperature (CPT and LRT) on

481 monthly scales particularly during July and August 2015 also discussed. To quantify the changes
482 that happened within the ASMA region, 11 years (2005-2015) of O_3, WV and CO observations
483 from the Aura-MLS data and 10 years (2006-2015) of tropopause temperature data from the
484 COSMIC RO temperature profiles are used. The NCEP-DOE Reanalysis 2 observed winds and
485 GPH data from 2005 to 2015 are also utilized. The results are obtained by comparing the trace gas
486 quantities in July and August 2015 with corresponding long-term monthly mean quantities.

487 The trace gases within the ASMA exhibit substantial anomalous behavior in July and August
488 2015. During July and August 2015, we observed an enhancement of O_3 and the lowering of CO
489 and WV over most of the ASMA region. The decrease of the tropospheric tracers (CO and WV) is
490 quite expected due to the weaker upward motions from the weak monsoon in 2015. This is
491 supported by a recent study reported by Fadnavis et al. (2019). They showed weaker upward
492 motions and deficient rainfall in the 2015 monsoon due to the strong El Niño conditions. However,
493 the strong enhancement in the stratospheric tracer (O_3) within the ASMA particularly over the
494 northeastern edges of the ASMA during July is quite interesting. This is might be due to the
495 stratospheric intrusions as well as transport from the mid-latitudes. Based on Fishman and Seiler
496 (1983), it was stated that the positive correlation between CO and O_3 indicates, the O_3 is produced
497 by in-situ in the troposphere whereas the correlation is negative means the O_3 originates from the
498 stratosphere. We noticed a strong negative correlation between CO and O_3 in the present study
499 with increased O_3 and decreased CO from the MLS measurements. This clearly reveals that the
500 observed increased O_3 within the ASMA during 2015 is the stratospheric origin. This is further
501 supported by higher negative GPH anomalies associated with a southward meandering of the
502 subtropical westerly jet over northeastern Asia in July (**Figs. 3** and **4**). Further, the increased O_3 at
503 100 hPa and 121 hPa over western edges of the ASMA during August clearly indicates the transport

of the O_3 towards outer regions through the outflow of the ASMA (**Fig. 7e-f**). Interestingly, the tropopause temperature obtained from the COSMIC RO data in July 2015 shows strong positive temperature anomalies (~5 K) over the entire ASMA region. These warm tropopause temperatures again supported the increased O_3 within the ASMA during 2015. The major findings obtained from the present study are summarized in the following.

- ❖ The spatial extension of the ASMA region shows higher than long-term mean except over northeastern Asia where it exhibits a strong southward shift in July. Whereas in August, the AMSA further separated into two anticyclones and the western Pacific mode anticyclone is clearly evident in August.
- ❖ The combination of Rossby wave breaking and pronounced southward meandering of subtropical westerlies play a crucial role on the dynamical and structural changes in the ASMA in 2015.
- ❖ Strong enhancement in O_3 at 100 hPa (>40%) is clearly evident within the ASMA and particularly higher over the northeastern edges of the ASMA in July. The enhanced O_3 is strongly associated with a dominant southward meandering of the subtropical westerlies. In August, the increased O_3 is significantly located over the western edges of the ASMA. This clearly indicates the transport from the ASMA to the edges through its outflow.
- ❖ A significant lowering of CO and WV within the ASMA is noticed during summer 2015. The lowering of WV is higher at 146 hPa than 100 hPa.
- ❖ Significant positive tropopause temperature anomalies (~5 K) is observed in the entire ASMA region in July whereas, in August, the strong positive anomalies are concentrated over the northeastern side of the ASMA.

The changes in the O_3 concentrations (increase/decrease) within the ASMA are one of the possible

mechanisms to strengthening/weakening of the ASMA (Braesicke et al., 2011). By using idealized climate model experiments, Braesicke et al. (2011) clearly demonstrated that the strengthening (weakening) of the ASMA occurred when the O_3 is decreased (increased) within the ASMA. The increased O_3 within the ASMA warms the entire anticyclone region and weakens the ASMA (Braesicke et al., 2011). Our results from the present study also in agreement with the results of Braesicke et al. (2011). We also observed a pronounced increase of O_3 within the ASMA associated with significant warming of tropopause as well as above and below the tropopause region in 2015. By using precipitation index, wind data and stream functions, previous studies reported that the ASMA circulation in 2015 was weaker than the normal (Tweedy et al., 2018; Yuan et al., 2019). Based on our present results, the strongly enhanced O_3 within the ASMA also might be one of the plausible reasons for weakening of the ASMA in 2015.

Author contributions: SRB designed the study, conducted research, performed initial data analysis and wrote the first manuscript draft. MVR, GB, SKP and NHL edited the first manuscript. All authors edited the paper.

Data Availability: All the data used in the present study is available freely from the respective websites. The MLS trace gases data obtained from Earth Science Data website. The NCEP_Reanalysis 2 data provided by the NOAA/OAR/ESRL PSL, Boulder, Colorado, USA, from their web site (http://www.cpc.ncep.noaa.gov/products/wesley/reanalysis2/kana/reanl2-1.htm) The COSMIC data is available from COSMIC CDAAC website (http://cdaac-www.cosmic.ucar.edu/cdaac/products.html).

Competing interests: The authors declare that they have no conflict of interest.

Acknowledgments: Aura MLS observations obtained from the GES DISC through their FTP site (https://mls.jpl.nasa.gov/index-eos-mls.php) is highly acknowledged. We thank the COSMIC Data

Analysis and Archive Centre (CDAAC) for providing RO data used in the present study through their FTP site (http://cdaac-www.cosmic.ucar.edu/cdaac/products.html). We also thank to NCEP/NCAR reanalysis for providing geopotential and wind data. We thank ECMWRF for providing ERA interim reanalysis data.

References

Anthes, R., Bernhardt, P., Chen, Y., Cucurull, L., Dymond, K., Ector, D., Healy, S., Ho, S., Hunt, D., Kuo, Y., Liu, H., Manning, K., Mccormick, C., Meehan, T., Randel, W., Rocken, C., Schreiner, W., Sokolovskiy, S., Syndergaard, S., Thompson, D., Trenberth, K., Wee, T., Yen, N., and Zeng, Z.: The COSMIC/FORMOSAT-3 – Mission early results, B. Am. Meteorol. Soc., 89, 313–333, 2008.

Avery, M. A., Davis, S. M., Rosenlof, K. H., Ye, H., Dessler, A. E., 2017. Large anomalies in lower stratospheric water vapour and ice during the 2015–2016 El Niño, Nat. Geosci., 10, 405–409, https://doi.org/10.1038/ngeo2961.

Basha, G., Ratnam, M. V., and Kishore, P.: Asian Summer Monsoon Anticyclone: Trends and Variability, Atmos. Chem. Phys. Discuss., https://doi.org/10.5194/acp-2019-668, in review, 2019.

Bergman, J. W., Fierli, F., Jensen, E. J., Honomichl, S., and Pan, L. L.: Boundary layer sources for the Asian anticyclone: Regional contributions to a vertical conduit, J. Geophys. Res.-Atmos., 118, 2560–2575, https://doi.org/10.1002/jgrd.50142, 2013.

Bian, J. C., Pan, L. L., Paulik, L., Vömel, H., and Chen, H. B.: In situ water vapor and ozone measurements in Lhasa and Kunming during the Asian summer monsoon, Geophys. Res. Lett., 39, L19808, https://doi.org/10.1029/2012GL052996, 2012.

Braesicke, P., O. J. Smith, P. Telford, and J. A. Pyle (2011), Ozone concentration changes in the Asian summer monsoon anticyclone and lower stratospheric water vapour: An idealised model study, Geophys. Res. Lett., 38, L03810, doi:10.1029/2010GL046228.

Diallo, M., Riese, M., Birner, T., Konopka, P., Müller, R., Hegglin, M. I., Santee, M. L., Baldwin, M., Legras, B., and Ploeger, F.: Response of stratospheric water vapor and ozone to the unusual timing of El Niño and the QBO disruption in 2015–2016, Atmos. Chem. Phys., 18, 13055–13073, https://doi.org/10.5194/acp-18-13055-2018, 2018.

579 Das, S.S., Suneeth, K.V., Ratnam, M.V., Girach, I. A., Das, S. K.: Upper tropospheric ozone
580 transport from the sub-tropics to tropics over the Indian region during Asian summer monsoon,
581 Clim Dyn., 52: 4567. https://doi.org/10.1007/s00382-018-4418-6, 2019.
582 Das, S., and Suneeth, K. V.: Seasonal and interannual variations of water vapor in the upper
583 troposphere and lower stratosphere over the Asian Summer Monsoon region- in perspective of
584 the tropopause and ocean-atmosphere interactions", Journal of Atmospheric and Solar-
585 Terrestrial Physics 201, 105244, doi:10.1016/j.jastp.2020.105244, 2020.
586 Dessler, A. E., Schoeberl, M. R., Wang, T., Davis, S. M., Rosenlof, K. H., and Vernier, J. P.:
587 Variations of stratospheric water vapor over the past three decades, J. Geophys. Res. Atmos.,
588 119, 12 588–12 598, doi:10.1002/2014JD021712, 2014.
589 Dunkerton, T. J.: The quasi-biennial oscillation of 2015–2016: Hiccup or death spiral? Geophys.
590 Res. Lett., 43, 10547–10552, https://doi.org/10.1002/2016GL070921, 2016.
591 Fadnavis, S. and Chattopadhyay, R.: Linkages of subtropical stratospheric intraseasonal intrusions
592 with Indian summer monsoon deficit rainfall, J. Climate, 30, 5083–5095,
593 https://doi.org/10.1175/JCLI-D-16-0463.1, 2017.
594 Fadnavis, S., Sabin, T.P., Roy, C. et al.: Elevated aerosol layer over South Asia worsens the Indian
595 droughts. Sci Rep 9, 10268, doi:10.1038/s41598-019-46704-9, 2019.
596 Fan, Q., Bian, J. and Pan, L. L.: Stratospheric entry point for upper-tropospheric air within the
597 Asian summer monsoon anticyclone, Sci. China Earth Sci., 60, 1685–
598 1693, https://doi.org/10.1007/s11430-016-9073-5, 2017.
599 Fishman, J., and Seiler, W.: Correlative nature of ozone and carbon monoxide in the troposphere
600 - Implications for the tropospheric ozone budget; J. Geophys. Res. 88,
601 https://doi.org/10.1029/JC088iC06p03662, 1983.
602 Fueglistaler, S., Dessler, A. E., Dunkerton, T. J., Folkins, I., Fu, Q., and Mote, P. W.: Tropical
603 Tropopause Layer, Rev. Geophys., 47, G1004+, https://doi.org/10.1029/2008RG000267, 2009.
604 Gadgil, S. and Francis, P. A.: El Niño and the Indian rainfall in June. Curr Sci 110:1010–1022,
605 2016.
606 Garny, H. and Randel, W. J.: Transport pathways from the Asian monsoon anticyclone to the
607 stratosphere, Atmos. Chem. Phys., 16, 2703–2718, https://doi.org/10.5194/acp-16-2703- 2016,
608 2016.
609 Gettelman, A., Randel, W. J., Massie, S., Wu, F.: El Niño as a natural experiment for studying the

610 tropical tropopause region, J. Clim., 14, 3375– 3392, 2001.
611 Gettelman, A., Kinnison, D. E., Dunkerton, T. J., and Brasseur, G. P.: Impact of monsoon
612 circulations on the upper troposphere and lower stratosphere, J. Geophys. Res.-Atmos., 109,
613 D22101, https://doi.org/10.1029/2004JD004878, 2004.
614 Highwood, E. J. and Hoskins, B. J.: The tropical tropopause, Q. J. Roy. Meteor. Soc., 124, 1579–
615 1604, https://doi.org/10.1002/qj.49712454911, 1998.
616 Ho, S.-P., Anthes, R. A., Ao, C.O., Healy, S., Horanyi, A., Hunt, D., Mannucci, A.J., Pedatella, N.,
617 Randel, W.J., Simmons, A., Steiner, A., Xie, F., Yue, X., Zeng., Z.: The
618 COSMIC/FORMOSAT-3 radio occultation mission after 12 years: Accomplishments,
619 remaining challenges, and potential impacts of COSMIC-2. Bull Amer Met Soc 100 online
620 version: https://journals.ametsoc.org/doi/pdf/10.1175/BAMS-D-18-0290.1
621 Honomichl, S. B., and Pan, L. L.: Transport from the Asian summer monsoon anticyclone over the
622 western Pacific. Journal of Geophysical Research: Atmospheres, 125, e2019JD032094.
623 https://doi.org/10.1029/2019JD032094, 2020.
624 Hossaini, R., Chipperfield, M., Montzka, M. P., Rap, S. A., Dhomse, S., and Feng, W.: Efficiency
625 of short-lived halogens at influencing climate through depletion of stratopsheric ozone, Nat.
626 Geosci., 8, 186–190, https://doi.org/10.1038/ngeo2363, 2015.
627 Jiang, J.H., Su, H., Zhai, C., Wu, L., Minschwaner, K., Molod, A.M., Tompkins, A.M.: An
628 assessment of upper troposphere and lower stratosphere water vapor in MERRA, MERRA2,
629 and ECMWF reanalyses using Aura MLS observations. J. Geophys. Res. Atmos. 120, 11.
630 https://doi.org/10.1002/2015JD023752, 468–11,485, 2015.
631 Kanamitsu, M., Ebisuzaki, W., Woollen, J., Yang, S.-K., Hnilo, J. J., Fiorino, M., and Potter, G. L.:
632 NCEP-DOE AMIP-II Renalalysys (R-2), B. Am. Meteorol. Soc., 83, 1631–1643,
633 https://doi.org/10.1175/BAMS-83-11-1631, 2002.
634 Khan, A., Jin, S.: Effect of gravity waves on the tropopause temperature, altitude and water vapor
635 in Tibet from COSMIC GPS Radio Occultation observations, J. Atmos. Sol. Terr. Phys. 138–
636 139, 23–31. https://doi.org/10.1016/j.jastp.2015.12.001, 2016.
637 Kim, J. and Son, S.-W.: Tropical Cold-Point Tropopause: Climatology, Seasonal Cycle, and
638 Intraseasonal Variability Derived from COSMIC GPS Radio Occultation Measurements, J.
639 Climate, 25, 5343–5360, https://doi.org/10.1175/JCLI-D-11-00554.1, 2012.

Kumar, K. K., Rajagopalan, B., Cane, M. A.: On the weakening relationship between the Indian monsoon and ENSO. Science 287:2156–2159, 1999.

Kursinski, E. R., Hajj, G. A., Schofield, J. T., Linfield, R. P., and Hardy, K. R.: Observing Earth's atmosphere with radio occultation measurements using the Global Positioning System, J. Geophys. Res., 102, 23429–23465, 1997.

Konopka, P., Ploeger, F., Tao, M., and Riese, M.: Zonally resolved impact of ENSO on the stratospheric circulation and water vapor entry values, J. Geophys. Res.-Atmos., 121, 11486–11501, https://doi.org/10.1002/2015JD024698, 2016.

Li, Q., Jiang, J. H., Wu, D. L., Read, W. G., Livesey, N. J., Waters, J. W., Zhang, Y., Wang,B., Filipiak, M. J., Davis, C. P., Turquety, S., Wu, S., Park, R. J., Yantosca, R. M., and Jacob, D. J.: Convective outflow of South Asian pollution: A global CTM simulation compared with EOS MLS observations, Geophys. Res. Lett., 32, L14 826, https://doi.org/10.1029/2005GL022762, 2005.

Li, D., Vogel, B., Müller, R., Bian, J., Günther, G., Li, Q., Zhang, J., Bai, Z., Vömel, H., and Riese, M.: High tropospheric ozone in Lhasa within the Asian summer monsoon anticyclone in 2013: influence of convective transport and stratospheric intrusions, Atmospheric Chemistry and Physics, 18, 17 979–17 994, https://doi.org/10.5194/acp-18-17979-2018, https://www.atmos-chem-phys.net/18/17979/2018/, 2018.

Livesey, N. J., Read, W. G., Wagner, P. A., Froidevaux, L., Lambert, A., Manney, G. L., Valle, L. F. M., Pumphrey, H. C., Santee, M. L., Schwartz, M. J., Wang, S., Fuller, R. A., Jarnot, R. F., Knosp, B. W., and Martinez, E.: Version 4.2x Level 2 data quality and description document, https://mls.jpl.nasa.gov/data/v4-2_data_quality_document.pdf, 2018

Nützel, M., Dameris, M., and Garny, H.: Movement, drivers and bimodality of the South Asian High, Atmos. Chem. Phys., 16, 14755–14774, https://doi.org/10.5194/acp-16-14755-2016, 2016.

Pan, L. L., Honomichl, S. B., Kinnison, D. E., Abalos, M., Randel, W. J., Bergman, J. W., and Bian, J. C.: Transport of chemical tracers from the boundary layer to stratosphere associated with the dynamics of the Asian summer monsoon, J. Geophys. Res.-Atmos., 121, 14159–14174, https://doi.org/10.1002/2016JD025616, 2016.

Park, M., Randel, W. J., Kinnison, D. E., Garcia, R. R., and Choi, W.: Seasonal variation of methane, water vapor, and nitrogen oxides near the tropopause: Satellite observations and

model simulations, J. Geophys. Res.-Atmos., 109, D03302, https://doi.org/10.1029/2003jd003706, 2004.

Park, M., Randel, W. J., Gettelman, A., Massie, S. T., and Jiang, J. H.: Transport above the Asian summer monsoon anticyclone inferred from Aura MLS tracers, J. Geophys. Res, 112, D16309, doi:10.1029/2006JD008294, 2007.

Park, M., Randel, W. J., Emmons, L. K., Bernath, P. F., Walker, K. A., and Boone, C. D.: Chemical isolation in the Asian monsoon anticyclone observed in Atmospheric Chemistry Experiment (ACE-FTS) data, Atmos. Chem. Phys., 8, 757–764, https://doi.org/10.5194/acp-8-757-2008, 2008

Park, M., Randel, W. J., Emmons, L. K., and Livesey, N. J.: Transport pathways of carbon monoxide in the Asian summer monsoon diagnosed from Model of Ozone and Related Tracers (MOZART), J. Geophys. Res., 114, D08303, https://doi.org/10.1029/2008JD010621, 2009.

Ramaswamy, C.: A preliminary study of the behavior of the Indian southwest monsoon in relation to the westerly jet-stream. Special Palmen No. Geophysica, 6, pp. 455-476, 1958.

Randel, W. J. and Park, M.: Deep convective influence on the Asian summer monsoon anticyclone and associated tracer variability observed with Atmospheric Infrared Sounder (AIRS), J. Geophys. Res., 111, D12314, https://doi.org/10.1029/2005jd006490, 2006.

Randel, W. J., Garcia, R. R., Calvo, N., and Marsh, D.: ENSO influence on zonal mean temperature and ozone in the tropical lower stratosphere, Geophys. Res. Lett., 36, L15822, https://doi.org/10.1029/2009GL039343, 2009.

Randel, W. J., Park, M., Emmons, L., Kinnison, D., Bernath, P., Walker, K. A., Boone, C., and Pumphrey, H.: Asian Monsoon Transport of Pollution to the Stratosphere, Science, 328, 611–613, https://doi.org/10.1126/science.1182274, 2010.

Rao, D.N., Ratnam, M.V., Mehta, S., Nath, D., Basha, G., Jagannadha Rao, V.V.M., et al: Validation of the COSMIC radio occultation data over gadanki (13. 48°N, 79.2°E): A tropical region, Terr J Atmos Ocean Sci 20, 59–70, https://doi.org/10.3319/TAO.2008.01.23.01(F3C), 2009.

RavindraBabu, S., VenkatRatnam, M., Basha, G., Krishnamurthy, B. V., and Venkateswararao, B.: Effect of tropical cyclones on the tropical tropopause parameters observed using COSMIC GPS RO data, Atmos. Chem. Phys., 15, 10239–10249, doi:10.5194/acp-15-10239-2015, 2015.

RavindraBabu, S., VenkataRatnam, M., Basha, G., Liou, Y.-A., Narendra Reddy, N.: Large Anomalies in the Tropical Upper Troposphere Lower Stratosphere (UTLS) Trace Gases Observed during the Extreme 2015–16 El Niño Event by Using Satellite Measurements, Remote Sensing. 2019, 11, 687.https://doi.org/10.3390/rs11060687, 2019. a

RavindraBabu, S., Venkat Ratnam, M., Basha, G., Krishnamurthy, B.V.: Indian summer monsoon onset signatures on the tropical tropopause layer. Atmos. Sci. Lett. 20, e884. https://doi.org/10.1002/asl.884, 2019. b

Ravindra Babu, S., Akhil Raj, S.T., Basha, G., Venkat Ratnam, M.: Recent trends in the UTLS temperature and tropical tropopause parameters over tropical South Indian region, J. Atmos. Solar Terr. Phys. 197:105164. https://doi.org/10.1016/j.jastp.2019.105164, 2020.

Ravindra Babu, S. and Liou, Y. A.: Tropical tropopause layer evolution during 2015–16 El Niño event inferred from COSMIC RO measurements, J. Atmos. Solar Terr. Phys. 212: 105507. https://doi.org/10.1016/j.jastp.2020.105507

Samanta, D., Dash, M. K., Goswami, B. N., and Pandey, P. C.: Extratropical anticyclonic Rossby wave breaking and Indian summer monsoon failure. Climate Dyn., 46, 1547–1562, doi:https://doi.org/10.1007/s00382-015-2661-7., 2016.

Santee, M. L., Manney, G. L., Livesey, N. J., Schwartz, M. J., Neu, J. L., and Read, W. G.: A comprehensive overview of the climatological composition of the Asian summer monsoon anticyclone based on 10 years of Aura Microwave Limb Sounder measurements, J. Geophys. Res.-Atmos., 122, 5491- 5514, https://doi.org/10.1002/2016jd026408, 2017.

Scherllin-Pirscher, B., Kirchengast, G., Steiner, A. K., Kuo, Y.-H., and Foelsche, U.: Quantifying uncertainty in climatological fields from GPS radio occultation: an empirical-analytical error model, Atmos. Meas. Tech., 4, 2019–2034, doi:10.5194/amt-4-2019-2011, 2011a.

Scherllin-Pirscher, B., Steiner, A. K., Kirchengast, G., Kuo, Y.-H., and Foelsche, U.: Empirical analysis and modeling of errors of atmospheric profiles from GPS radio occultation, Atmos. Meas. Tech., 4, 1875–1890, doi:10.5194/amt-4-1875-2011, 2011b.

Sprenger, M., Maspoli, M. C., and Wernli, H.: Tropopause folds and cross-tropopause exchange: A global investigation based upon ECMWF analyses for the time period March 2000 to February 2001, J. Geophys. Res., 108, 8518, https://doi.org/10.1029/2002JD002587, 2003.

730 Škerlak, B., Sprenger, M., and Wernli, H.: A global climatology of stratosphere–troposphere
731 exchange using the ERA-Interim data set from 1979 to 2011, Atmos. Chem. Phys., 14, 913–
732 937, https://doi.org/10.5194/acp-14-913-2014, 2014.
733 Tweedy, O. V., Waugh, D. W., Randel, W. J., Abalos, M., Oman, L. D., and Kinnison, D. E.: The
734 Impact of Boreal Summer ENSO Events on Tropical Lower Stratospheric Ozone, Journal of
735 Geophysical Research: Atmospheres, 123, 9843–9857, https://doi.org/10.1029/2018JD029020.
736 Uppala, S. M., Kållberg, P. W., Simmons, A. J., Andrae, U., da Costa Bechtold, V., Fiorino, M.,
737 Gibson, J. K., Haseler, J., Hernandez, A., Kelly, G. A., Li, X., Onogi, K., Saarinen, S., Sokka,
738 N., Allan, R. P., Andersson, E., Arpe, K., Balmaseda, M. A., Beljaars, A. C. M., van de Berg,
739 L., Bidlot, J., Bormann, N., Caires, S., Chevallier, F., Dethof, A., Dragosavac, M., Fisher, M.,
740 Fuentes, M., Hagemann, S., Hólm, E., Hoskins, B. J., Isaksen, L., Janssen, P. A. E. M., Jenne,
741 R., McNally, A. P., Mahfouf, J. F., Morcrette, J. J., Rayner, N. A., Saunders, R. W., Simon, P.,
742 Sterl, A., Trenberth, K. E., Untch, A., Vasiljevic, D., Viterbo, P., and Woollen, J.: The ERA-40
743 re-analysis, Q. J. Roy. Meteor. Soc., 131, 2961–3012, https://doi.org/10.1256/qj.04.176, 2005.
744 Vellore, R. K., Kaplan, M. L., and Krishnan, R., et al.: Monsoon-extratropical circulation
745 interactions in Himalayan extreme rainfall; *Clim. Dyn.* **46,** 3517, 2016.
746 https://doi.org/10.1007/s00382-015-2784-x.
747 Venkat Ratnam, M., Ravindra Babu, S., Das, S. S., Basha, G., Krishnamurthy, B. V., and
748 Venkateswararao, B.: Effect of tropical cyclones on the stratosphere–troposphere exchange
749 observed using satellite observations over the north Indian Ocean, Atmos. Chem. Phys., 16,
750 8581–8591, https://doi.org/10.5194/acp-16-8581-2016, 2016.
751 Vernier, J.-P., Thomason, L. W., and Kar, J.: CALIPSO detection of an Asian tropopause aerosol
752 layer, Geophys. Res. Lett., 38, L07804, https://doi.org/10.1029/2010GL046614, 2011
753 Vernier, J.-P., Fairlie, T. D., Deshler, T., Ratnam, M. V., Gadhavi, H., Kumar, B. S., Natarajan,
754 M., Pandit, A. K., Raj, S. T. A., Kumar, A. H., Jayaraman, A., Singh, A. K., Rastogi, N., Sinha,
755 P. R., Kumar, S., Tiwari, S., Wegner, T., Baker, N., Vignelles, D., Stenchikov, G., Shevchenko,
756 I., Smith, J., Bedka, K., Kesarkar, A., Singh, V., Bhate, J., Ravikiran, V., Rao, M. D.,
757 Ravindrababu, S., Patel, A., Vernier, H., Wienhold, F. G., Liu, H., Knepp, T. N., Thomason,
758 L., Crawford, J., Ziemba, L., Moore, J., Crumeyrolle, S., Williamson, M., Berthet, G., Jégou,
759 F., and Renard, J.- B.: BATAL: The balloon measurement campaigns of the Asian tropopause

760 aerosol layer, B. Am. Meteorol. Soc., 99, 955–973, https://doi.org/10.1175/BAMS-D-17-
761 0014.1, 2018.
762 Vogel, B., Günther, G., Müller, R., Grooß, J.-U., Afchine, A., Bozem, H., Hoor, P., Krämer, M.,
763 Müller, S., Riese, M., Rolf, C., Spelten, N., Stiller, G. P., Ungermann, J., and Zahn, A.:
764 Longrange transport pathways of tropospheric source gases originating in Asia into the northern
765 lower stratosphere during the Asian monsoon season 2012, Atmos. Chem. Phys., 16, 15301–
766 15325, https://doi.org/10.5194/acp-16-15301-2016, 2016.
767 Wang, B., Xiang, B., Li, J., Webster, P. J., Rajeevan, M. N., Liu, J., Ha, K. –J.: Rethinking Indian
768 monsoon rainfall prediction in the context of recent global warming. Nat Commun 6:7154.
769 doi:10.1038/ncomms8154, 2015.
770 Xu, X., Zhao, T., Lu, C., Guo, Y., Chen, B., Liu, R., Li, Y., Shi, X.: An important mechanism
771 sustaining the atmospheric "water tower" over the Tibetan Plateau. Atmos. Chem. Phys. 14,
772 11287–11295. https://doi.org/10.5194/acp-14-11287- 2014.
773 Yan, R.-C., Bian, J.-C., and Fan, Q.-J.: The Impact of the South Asia High Bimodality on the
774 Chemical Composition of the Upper Troposphere and Lower Stratosphere, Atmos. Ocean. Sci.
775 Lett., 4, 229–234, 2011.
776 Yan, R. C. and Bian, J. C.: Tracing the boundary layer sources of carbon monoxide in the Asian
777 summer monsoon anticyclone using WRF–Chem, Adv. Atmos. Sci., 32, 943–951,
778 https://doi.org/10.1007/s00376-014-4130-3, 2015.
779 Yan, X., Konopka, P., Ploeger, F., Tao, M., Müller, R., Santee, M. L., Bian, J., and Riese, M.: El
780 Niño Southern Oscillation influence on the Asian summer monsoon anticyclone, Atmospheric
781 Chemistry and Physics, pp. 8079–8096, https://doi.org/10.5194/acp-18-8079-2018, 2018.
782 Yu, P., Rosenlof, K. H., Liu, S., Telg, H., Thornberry, T. D., Rollins, A. W., Portmann, R. W., Bai,
783 Z., Ray, E. A., Duan, Y., Pan, L. L., Toon, O. B., Bian, J., and Gao, R.-S.: Efficient transport of
784 tropospheric aerosol into the stratosphere via the Asian summer monsoon anticyclone,
785 Proceedings of the National Academy of Sciences, pp. 6972–6977,
786 https://doi.org/10.1073/pnas.1701170114, 2017.
787 Yuan, C., Lau, W. K. M., Li, Z., and Cribb, M.: Relationship between Asian monsoon strength and
788 transport of surface aerosols to the Asian Tropopause Aerosol Layer (ATAL): interannual
789 variability and decadal changes, Atmos. Chem. Phys., 19, 1901-1913,
790 https://doi.org/10.5194/acp-19-1901-2019, 2019.